

Going, going, gone dark: Quantifying the Scatter in the Faintest Dwarf Galaxies

Ferah Munshi^{1,2}, Alyson M. Brooks¹, Elaad Applebaum¹, Daniel R. Weisz³, Fabio Governato⁴, Thomas R. Quinn⁴

¹*Department of Physics & Astronomy, Rutgers, The State University of New Jersey, 136 Frelinghuysen Rd, Piscataway, NJ 08854;*

²*Department of Physics and Astronomy, Vanderbilt University, PMB 401807, Nashville, TN 37206;*

³*Department of Astronomy, 501 Campbell Hall #3411, University of California at Berkeley, Berkeley, CA 94720-3411*

⁴*Department of Astronomy, University of Washington, Box 351580, Seattle, WA 98195-1580;*

May 19, 2017

ABSTRACT

We predict the stellar mass-halo mass (SMHM) relationship for dwarf galaxies and their satellites residing in halos down to $M_{\text{halo}} = 10^7 M_{\odot}$ with $10^4 M_{\odot} < M_{\text{star}}(z=0) < 10^8 M_{\odot}$, and quantify the predicted scatter in the relation at the low mass end, using cosmological simulations. The galaxies were drawn from a cosmological simulation run with the N-body + SPH code, ChaNGA, at a high resolution of 60 pc. For $M_{\text{halo}} > 10^9 M_{\odot}$, the simulated SMHM relationship agrees with literature determinations, including exhibiting a small scatter. However, the scatter in the SMHM relation increases dramatically for lower-mass halos. We find that some of this scatter is due to *dark dwarfs*, halos devoid of stars. However, even when only considering well-resolved halos that contain a stellar population, the scatter in stellar mass reaches nearly 1 dex for $M_{\text{halo}}(z=0) 10^7 M_{\odot}$. Much of this scatter is due to including satellites of the dwarf galaxies that have had their halo masses reduced through tidal stripping. The fraction of dark dwarfs (those that contain no stars) increases substantially with decreasing halo mass. When these dark halos are considered, the true scatter in the SMHM at low masses is even larger. At the faintest end of the SMHM relation probed by our simulations, a galaxy cannot be assigned a unique halo mass based solely on its luminosity. We provide a formula to stochastically populate low-mass halos following our results. Our predicted large scatter at low halo masses increases the slope of the resulting stellar mass function on the ultra-faint dwarf galaxy scales currently being probed by such surveys as the Dark Energy Survey or the Hyper-Suprime Cam Subaru Strategic Program, and in the future by the Large Synoptic Survey Telescope.

Key words: galaxies: dwarf – galaxies: haloes – galaxies: formation

1 INTRODUCTION

In the Λ Cold Dark Matter (Λ CDM) paradigm of cosmological structure formation, dwarf galaxies are predicted to be the smallest, most abundant, yet least luminous systems in the Universe. Recent attempts to link dwarf galaxies to their parent dark matter halos via abundance matching have led to discrepancies between theory and observations (e.g., Ferrero et al. 2012; Garrison-Kimmel et al. 2014a; Papastergis et al. 2015; Brook & Di Cintio 2015). Abundance matching quite literally matches a stellar mass or luminosity at a given abundance to dark matter halos with the same abundance, derived from a dark matter-only simulation. A monotonic relationship is generally

assumed (Guo et al. 2010; Behroozi, Wechsler & Conroy 2013; Moster, Naab & White 2013). For halos of roughly Milky Way mass and greater, abundance matching also reproduces clustering statistics (e.g., Conroy & Wechsler 2009, and references within). Additionally, numerous abundance matching studies yield fair agreement for the stellar mass-to-halo mass relation (SMHM) for halos of masses $\gtrsim 10^{11} M_{\odot}$.

However, derivations of the SMHM at lower masses have yielded discrepancies (e.g., Moster, Naab & White 2013; Behroozi, Wechsler & Conroy 2013; Brook et al. 2014; Garrison-Kimmel et al. 2014b). If the SMHM has the form $M_{\text{star}} \propto M_{\text{halo}}^{\alpha}$, the range of derived α varies from 1.6 – 3.1

for low mass galaxies. Moster, Naab & White (2013) and Behroozi, Wechsler & Conroy (2013) did not have data in order to derive the SMHM relation below stellar masses of a few $\times 10^7 M_\odot$. While their results from higher masses should obviously not be extrapolated to lower masses, the slopes at their lowest measured mass were quite different, $\alpha = 1.4$ (Behroozi, Wechsler & Conroy 2013) versus $\alpha = 2.4$ (Moster, Naab & White 2013). Brook et al. (2014) and Garrison-Kimmel et al. (2014b), on the other hand, used Local Group galaxy data to determine the SMHM relation at $10^6 < M_{star}/M_\odot < 10^8$. Again, they came to quite different conclusions about the value of α , 3.1 in Brook et al. (2014) and 1.9 in Garrison-Kimmel et al. (2014b).¹ Read et al. (2017) find a shallower stellar mass function below $10^9 M_\odot$, $\alpha = 1.6$, and attribute this to that fact that they use a strictly isolated galaxy sample, arguing that including galaxies processed in a group environment leads to a steeper SMHM relation.

The relative agreement in the SMHM relation at the high mass end also points to the fact that the scatter at the high mass end is consistently measured to be relatively small, 0.2 dex or less (Behroozi, Wechsler & Conroy 2013; Reddick et al. 2013; Kravtsov, Vikhlinin & Meshcheryakov 2014; Matthee et al. 2017). However, the scatter at the low mass end may be much larger. In fact, the star formation history at dwarf galaxy scales is likely to depend on the mass accretion history of the halo (Brooks & Zolotov 2014; Weisz et al. 2015; Sawala et al. 2016), and observations indicate that dwarf galaxies over a range of stellar masses may all occupy dark matter halos with a narrow range of mass (e.g., see Figure 1 of Klypin et al. 2015; Ferrero et al. 2012; Strigari et al. 2008). Garrison-Kimmel et al. (2016) explored the implications of scatter within M_{star} at a given M_{halo} using Local Group data down to $M_{star} \sim 10^5 M_\odot$. They demonstrated that there is a degeneracy between the slope and the scatter of the SMHM when using the SMHM to derive the stellar mass function. Small halos are more likely to scatter to large stellar masses due to the rapidly rising mass function. Hence, large scatter requires a steeper SMHM slope in order to reproduce the observed stellar mass function.

Related, it is also possible that low mass halos may be entirely devoid of stars, or contain so few as to be beyond detection (e.g., O’Shea et al. 2015). Even if one considers scatter in the SMHM relation, it is common in abundance matching to assume that all halos continue to host galaxies. In reality, at low halo masses, one halo may contain a faint galaxy, while another halo at the same mass is entirely devoid of stars. Galaxies that form early are more concentrated (Wechsler et al. 2002; Zhao et al. 2003). For those galaxies with low concentration, reionization may stifle star formation entirely (e.g., Gnedin 2000; Governato et al. 2007; Okamoto, Gao & Theuns 2008; Brown et al. 2012; Brooks et al. 2013; Brown et al. 2014; Weisz et al. 2014). Sawala et al. (2015) used simulations representative of the Local Group to show that the fraction of halos which are unpopulated (not luminous) increases drastically at halo

masses less than $10^8 M_\odot$, suggesting a plummeting galaxy formation efficiency at these mass scales.

A number of simulators have used baryonic simulations to show that they match the derived SMHM at halo masses above $10^{10} M_\odot$ (e.g., Brook et al. 2012; Aumer et al. 2013; Hopkins et al. 2013; Munshi et al. 2013), but only a few have examined the SMHM of simulated dwarf galaxies below this mass (Munshi et al. 2013; Shen et al. 2014; Oñorbe et al. 2015; Sawala et al. 2015). Sawala et al. (2015) studied a larger population of dwarfs than the other works, tracing halos down to $\sim 10^8 M_\odot$. They showed that an abundance matching that used only *populated* halos leads to placing higher stellar mass galaxies into halos than traditional abundance matching, i.e., it alters the slope of the SMHM relation at low masses. However, almost all of these low mass halos were satellite galaxies, which may have earlier formation times than field galaxies and be more luminous at a fixed halo mass (Brooks & Zolotov 2014; Sawala et al. 2016). We demonstrate in this work that the characteristic “bend” in the SMHM at low halo masses found by Sawala et al. (2015) is a feature that arises due to the inclusion of satellite galaxies in the SMHM relation.

In this paper we address the question: for every low mass dark matter halo, how do stars populate it? We do this using a simulated zoomed-in region that contains many dwarfs. We examine both field dwarfs and their satellites, down to lower masses than previously studied. We show that, for many low mass halos, there are potentially no stars that inhabit them. These halos could have masses of $0 M_\odot$, and are “dark halos.” We both quantify the occupation fraction of dwarf galaxy halos in an Λ CDM framework as a function of decreasing halo mass, and quantify the scatter in the stellar mass at a given halo mass in the faintest dwarfs.

By quantifying the occupation fraction, slope, and scatter of the SMHM relation, we provide a tool for modelers to populate low mass halos. This allows us to predict the stellar mass function of dwarf galaxies. We show that the stellar mass function increases in slope in the stellar mass range of ultra-faint dwarf galaxies ($10^3 \lesssim M_{star}/M_\odot \lesssim 10^5$). A number of satellites have recently been discovered in this mass range, thanks to the efforts of the ATLAS (Torrealba et al. 2016), *Dark Energy Survey* (DES, Bechtol et al. 2015; Drlica-Wagner et al. 2015; Kim & Jerjen 2015; Kim et al. 2015; Kuposov et al. 2015; Luque et al. 2017), *Hyper Suprime-Cam Subaru Strategic Program* (HSC-SSP, Homma et al. 2017), *Magellanic Satellites Survey* (MagLiteS, Drlica-Wagner et al. 2016), *Survey of the Magellanic Stellar History* (SMASH, Martin et al. 2015), and *PanSTARRs* (Laevens et al. 2015) surveys. More ultra-faint dwarfs are likely to be found in the coming years from these same surveys, and when the *Large Synoptic Survey Telescope* (LSST) comes online (Tollerud et al. 2008). Additionally, searches for satellites around dwarf galaxies may also find new ultra-faint dwarfs (Dooley et al. 2016). Hence, by studying the low mass end of the SMHM relation, we are able to make predictions about this population of new galaxies that are being discovered.

It is the recent success of simulations in matching dwarf galaxy properties (e.g., Governato et al. 2010; Brooks & Zolotov 2014; Shen et al. 2014) that allow us to undertake this work. At the dwarf galaxy scale, the different slopes between the observed galaxy stellar mass function and

¹ Though the slope is dependent on the normalization at higher masses, and the values come into better agreement when a consistent normalization is adopted, see Garrison-Kimmel et al. (2016).

the Λ CDM predicted halo mass function require that galaxies at halo masses below $10^{11} M_{\odot}$ have gas cooling and star formation efficiencies much lower than those of Milky-Way sized galaxies. While this trend was historically difficult to produce in cosmological simulations, recent high resolution cosmological simulations that resolve scales on the order of giant molecular clouds can include more realistic models for star formation and feedback, resulting in simulations that can successfully reproduce the observed trends in star formation efficiency (Hopkins et al. 2013; Aumer et al. 2013; Brook et al. 2012; Munshi et al. 2013; Stinson et al. 2013; Simpson et al. 2013; Governato et al. 2015; Wheeler et al. 2015; Christensen et al. 2016; Fitts et al. 2016). The success of models in reproducing reliable and accurate dwarf galaxies lies in the ability to be able to resolve the impact of baryonic processes on the interstellar medium and star formation (Munshi et al. 2014). When this happens, the simulations also simultaneously reproduce additional observed trends in dwarf galaxies, such as cored dark matter density profiles (Governato et al. 2012; Pontzen & Governato 2014; Di Cintio et al. 2014; Maxwell, Wadsley & Couchman 2015; Oñorbe et al. 2015; Read, Agertz & Collins 2016) and bulge disks (Brook et al. 2011; Brooks & Christensen 2016).

In this paper we predict the fraction of small dark matter halos that should host galaxies, and what scatter the stochasticity of star formation and mass loss of satellites after infall add to the relationship between stellar mass and halo mass. We do so with simulations that, a priori, require no further tuning to successfully match observed properties, including published mass-metallicity relationships (Brooks et al. 2007; Christensen et al. 2016), cold gas fractions (Munshi et al. 2013; Brooks et al. 2017) and dark matter profile shapes (Governato et al. 2010; Christensen et al. 2014). The inclusion of realistic feedback models, combined with increasing detail and resolution, is key to understanding the complex interdependency between different types of feedback and the formation of dwarf galaxies as they look today. We discuss these simulations in Section 2. In Section 3 we show that, at the lowest halo masses, there no longer is a strict stellar mass-to-halo mass relationship, with the scatter in stellar mass increasing by an order of magnitude over a two decade decrease in halo mass. We also quantify the occupation fraction of dark matter halos as a function of declining halo mass. We quantify the slope and scatter of the SMHM relation. We summarize our results in Section 4.

2 SIMULATIONS

The simulations used in this work are run with the N-Body + SPH code CHANGA (Menon et al. 2015) in a fully cosmological Λ CDM context using WMAP Year 3 cosmology: $\Omega_0 = 0.26$, $\Lambda = 0.74$, $h = 0.73$, $\sigma_8 = 0.77$, $n = 0.96$. CHANGA adopts all the same physics modules as in our previous code, GASOLINE, but utilizes the CHARM++ run-time system for dynamic load balancing and computation/communication overlap in order to effectively scale up the number of cores. As described in Keller et al. (2014), CHANGA has improved its SPH implementation in order to more realistically model the gas physics at the hot-cold interface. The developers of CHANGA are part of the AGORA collaboration, which will

compare the implementation of hydrodynamics across cosmological codes (Kim et al. 2014).

The galaxy sample utilized in this manuscript is selected from a uniform dark matter-only simulation of 25 Mpc per side. From this volume, a field-like region was selected, representing a cosmological “sheet.” It was then resimulated at extremely high resolution using the “zoomed-in” volume renormalization technique (Katz & White 1993; Pontzen et al. 2008). The zoom-in technique allows for very high resolution, while accurately capturing the tidal torques from large scale structure that deliver angular momentum to galaxy halos (Barnes & Efstathiou 1987). These zoom-in simulations have a hydrodynamical smoothing length as small as 6 pc, a gravitational force softening of 60 pc, and equivalent resolution to a 4096^3 grid. Dark matter particles have a mass of $6650 M_{\odot}$, while gas particles begin with a mass of $1410 M_{\odot}$, and star particles are born with 30% of their parent gas particle mass. This sample represents a large number of some of the highest resolution published simulated cosmological dwarf galaxies. We give this set of simulated galaxies the nickname “The 40 Thieves.”

This set of simulations includes metal line cooling and the diffusion of metals (Shen, Wadsley & Stinson 2010) as well as the non-equilibrium abundances of H and He. We apply a uniform, time-dependent UV field from Haardt & Madau (2012) in order to model photoionization and heating. Additionally, we adopt a simple model for self-shielding following the models of Pontzen et al. (2010). Star formation is modeled based on a gas density threshold comparable to the mean density of molecular clouds and is similar to that described in Governato et al. (2010). Simply, star formation occurs stochastically when gas particles become cold ($T < 10^4$ K) and when gas reaches a density threshold of 100 amu/cc. At this threshold, star formation follows a Schmidt Law, as described in Governato et al. (2010). Governato et al. (2015) showed that this star formation model (*g3* in that paper) leads to a bursty but continuous star formation history (SFH), and generated mock color-magnitude diagrams to confirm in observation-space that a dwarf galaxy at the same resolution as the dwarf galaxies in this paper matches observed resolved stellar populations. Models that were bursty, but without an underlying continuous SFH, are not consistent with the observations.

We adopt the “blastwave” supernova feedback approach (Stinson et al. 2006), in which mass, thermal energy, and metals are deposited into nearby gas when massive stars evolve into supernovae. The thermal energy deposited amongst those nearby gas neighbors is 10^{51} ergs per supernova event. Subsequently, gas cooling is turned off until the end of the momentum-conserving phase of the supernova blastwave. Note that, unlike some other sub-grid feedback schemes (e.g., Oppenheimer et al. 2010; Marinacci, Pakmor & Springel 2014), this model keeps gas hydrodynamically coupled at all times. The coupling of 10^{51} ergs of energy into the interstellar medium, combined with the turning off of cooling in the affected gas particles, is designed to mimic the effect of energy deposited in the local ISM by *all* processes related to young stars, including UV radiation from massive stars (see Agertz et al. 2013).

Individual halos are identified using AMIGA’S

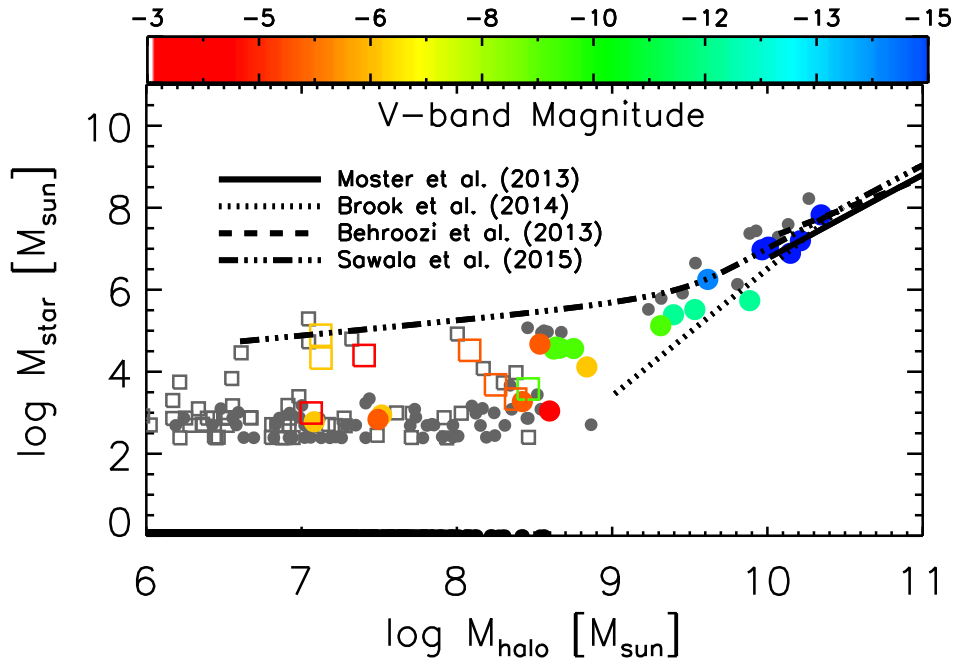


Figure 1. *Stellar Mass versus Halo Mass.* Results from galaxies in the 40 Thieves simulation are compared to various published SMHM relations. We show well-resolved galaxies ($M_{\text{halo}} > 10^7 M_{\odot}$) in color, with each galaxy color coded by its absolute V -band magnitude, as indicated in the color bar. For these well-resolved halos, we calculate their stellar mass based on their photometric colors and use the halo mass of their corresponding counterparts in a dark matter-only run (see Munshi et al. 2013). The grey points are instead results directly from the baryonic run, and include all halos that host at least one star particle. The black points along $\log(M_{\text{star}}) = 0$ are halos that contain no stars. Open squares indicate satellite galaxies, while filled circles represent central galaxies. Our simulations are consistent with all relations at halo masses above $10^{10} M_{\odot}$, but the scatter in the relation increases with decreasing halo mass. Below $\sim 10^9 M_{\odot}$, there is no single stellar to halo mass relationship for the simulated dwarfs.

HALO FINDER² (AHF, Gill, Knebe & Gibson 2004; Knollmann & Knebe 2009). The virial radius is defined to be the radius for which the average halo density is some multiple of the background density, following an overdensity criterion that varies with redshift Bryan & Norman (1998). At $z = 0$, the virial radius is defined as the radius within which the average halo density is approximately equal to 100 times the critical density. For satellites in this work, we trace back the main progenitor to find the maximum halo mass that the halo attained. At each snapshot, the main progenitor is defined to be the halo in the previous step that contains the majority of the particles in the current halo.

3 RESULTS

In Figure 1, we show the stellar mass of the simulated galaxies in the 40 Thieves as a function of halo mass. Also plotted are various published SMHM relations that were derived at higher masses (Moster, Naab & White 2013; Brook et al. 2014; Behroozi, Wechsler & Conroy 2013;

Sawala et al. 2015). In this Figure, the colored points are only those halos with $M_{\text{halo}} > 10^7 M_{\odot}$ and $M_{\text{star}} > 600 M_{\odot}$. This halo mass corresponds to the hydrogen cooling limit, and focusing on halos greater than this mass ensures that our dark matter halos are sufficiently well-resolved (more than 1500 particles). For the colored points, the stellar masses in Figure 1 are calculated using each simulated galaxy’s photometric color, as described in Munshi et al. (2013). The plotted halo masses are taken from a dark matter-only simulation of the same galaxies in order to be consistent with the fact that the derived SMHM relations that we compare to at the high mass end used mass functions from dark matter-only simulations. The small grey points are instead the results for the same halos if the values are taken from the baryonic runs, summing both the stellar and dark matter particle masses, and also including all halos with at least one star particle, regardless of halo mass. Open squares indicate satellite galaxies, while filled circles represent central galaxies. The black points along $\log(M_{\text{star}}) = 0$ are halos that contain no stars.

Simulated galaxies shown as colored points in Figure 1 are color coded by their V -band magnitude.³ This color cod-

² AHF is available for download at <http://popia.ft.uam.es/AHF/Download.html>.

³ The V -band magnitude is calculated in *pynbody* (Pontzen et al. 2013), which utilizes the Padova simple stellar population

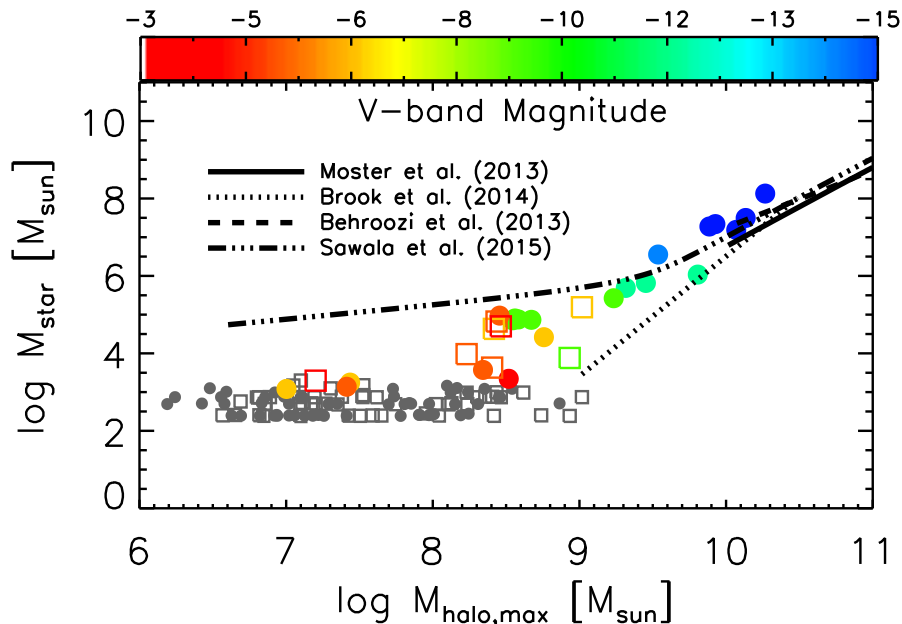


Figure 2. *Stellar Mass versus Maximum Halo Mass.* Similar to Figure 1 except that satellite galaxies at $z = 0$ are now shown at the time of their maximum halo mass, and the stellar mass at that corresponding time. Central galaxies are as in Figure 1, except that all results are now taken from the baryonic simulations (e.g., we do not use the corresponding dark matter-only halo mass nor do we use photometrically derived stellar masses). Again, grey points include all halos, even those that are not well resolved, and open squares indicate satellite galaxies, while filled circles represent central galaxies. Compared to Figure 1, it is clear that adopting the maximum halo mass decreases the scatter at the low mass end.

ing helps to emphasize that the 40 Thieves sample includes a wide range of stellar populations and star formation histories, from bright dwarfs to ultra-faint dwarfs.

At the faintest end of the SMHM relation probed by the 40 Thieves, a galaxy cannot be assigned a unique halo mass based solely on its luminosity. For example, as shown in Figure 1, a galaxy as bright as $M_V \sim -7$ can be hosted by halo masses that span roughly two orders of magnitude, ranging from $\sim 10^7 M_\odot$ to $\sim 10^9 M_\odot$. This is in stark contrast to conventional abundance matching, which assumes there exists a one-to-one relationship between luminosity (or stellar mass) and halo mass.

Figure 1 demonstrates that, as halo masses decline, the scatter in the stellar masses of the 40 Thieves drastically increases. However, Figure 2 emphasizes that the scatter at the lowest masses ($M_{halo} \sim 10^7 M_\odot$) can be attributed to including satellites of the dwarf galaxies in the relation. Figure 2 shows the maximum halo mass of satellites (typically at a time just before infall onto their parent halo), and the stellar mass at that time. Similarly, the $z = 0$ SMHM relation of Sawala et al. (2015) is dominated by satellite galaxies at the low mass end.

Although the most massive central dwarf in our simulation is comparable in mass to the SMC, it has one satellite with $M_{star} \sim 1000 M_\odot$. In fact, the six most massive central dwarfs in the simulation each contain at least one satellite

brighter than $M_V = -4$, while one galaxy has two, for a total of eight well-resolved satellites shown in Figures 1 and 2. The stellar masses (halo masses) of the parent dwarf galaxies range from $10^6 - 10^8 M_\odot$ ($6 \times 10^9 - 2 \times 10^{10} M_\odot$).

Considering the maximum halo mass for the satellites reduces the scatter in stellar mass at the lowest halo masses, from ~ 1 dex to ~ 0.25 dex at $M_{halo} \sim 10^7 M_\odot$. In some cases subhalos lose more than an order of magnitude in halo mass after infall. The halos with $M_{star} \sim 10^4 M_\odot$ and $M_{halo} \sim 10^7 M_\odot$ in Figure 1 are satellites that originally had $M_{halo} > 10^8 M_\odot$ and have been substantially stripped of mass after infall. Stellar masses are more robust, and only those halos with significant halo stripping have lost about a factor of two in stellar mass. This is consistent with earlier findings that $\sim 90\%$ of the dark matter mass can be stripped before stars are stripped (Peñarrubia, McConnachie & Navarro 2008; Libeskind et al. 2011; Muñoz, Majewski & Johnston 2008; Chang, Macciò & Kang 2013; Brooks & Zolotov 2014).

3.1 Quantifying the Scatter

In this section we quantify the scatter in our SMHM relation. We use the $z = 0$ results for halo masses of the satellites. Previous constraints on the low mass end of the SMHM relation use galaxies drawn from the Local Volume to derive a stellar mass function (Brook et al. 2014; Garrison-Kimmel et al. 2014b), including satellite galaxies. Hence, the adopted halo mass functions should not discriminate between satellites and centrals.

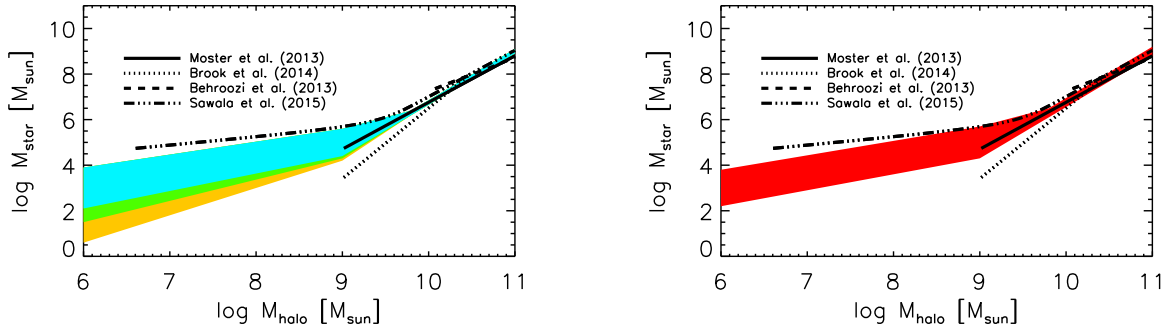


Figure 3. *Left Panel: Scatter in stellar mass at a given halo mass at $z = 0$ with various stellar mass cuts. Right Panel: Scatter in halo mass at a given stellar mass.* Lines are a sample of published SMHM relationships. Colored shaded regions are bounded by mean scatter in a given mass bin. Cyan shading represents scatter from well-resolved halos, green shading represents the increased scatter from halos that contain one star particle or more, and orange shading represents increased scatter by including dark halos.

3.1.1 Well-resolved Halos

Figure 3 shows the range of scatter in our simulated SMHM relation. We adopt log-normal scatter. The left plot shows the scatter in $\log(M_{star})$ at a fixed halo mass, while the right plot shows the scatter in $\log(M_{halo})$ at a fixed stellar mass. The cyan band in the left panel shows the scatter for all of the well-resolved halos that are shown in Figure 1 (below we discuss the scatter when all luminous halos are included, and when dark halos are included as well). At a given halo mass, the scatter in stellar mass is of order 0.1 dex for halos more massive than $\sim 10^9 M_{\odot}$. The scatter in stellar mass increases to 0.9 dex at the smallest halo masses for these well-resolved halos. In the right hand panel, the scatter in halo mass at a given stellar mass is shown by the red band. For stellar masses greater than $10^{5.5} M_{\odot}$, the scatter in halo mass is of order 0.2 dex, while the scatter is 0.7 dex at lower stellar masses.

As noted in the Introduction, Garrison-Kimmel et al. (2016) recently demonstrated the impact of scatter in the SMHM relation on the resulting stellar mass function. They explored both a model in which the scatter is constant as a function of halo mass, and a model in which the scatter increases as halo mass declines. Clearly, our results favor a model in which the scatter increases toward low halo masses. Garrison-Kimmel et al. (2016) quantify the increasing scatter as follows:

$$\sigma = 0.2 + \gamma(\log_{10}M_{halo} - \log_{10}M_1) \quad (1)$$

where σ is the scatter, γ is the rate as which the scatter grows, and M_1 is a characteristic mass above which the scatter remains constant. Munshi et al. (2013) demonstrated that our simulations are in good agreement with the derived SMHM of Moster, Naab & White (2013) at the high mass end, i.e., a slope of the SMHM $\alpha = 2.4$. This slope continues to fit our results down to $\log(M_{halo}) = 8.4$. Below this halo mass, we must define a new, shallower slope in order to fit the trend of the well-resolved halos, $\alpha = 0.64$. Our scatter remains roughly constant (and small) above $M_1 = 5 \times 10^9 M_{\odot}$, and grows below this halo mass. Using Eqn. 1 with the well-resolved simulated galaxies yields $\gamma = -0.26$.

3.1.2 All Populated Halos

We next loosen our restriction from all well-resolved halos to halos that contain one or more star particles. The grey points in Figure 1 show results for all halos in the simulation that contain stars. Note that in this case, we drop our calculation of stellar masses according to photometric color, and our assignment of halo mass based on the dark matter-only run. That is, the grey points in Figure 1 are direct from our baryonic simulation results, including for the halos that were also in our well-resolved sample. Our stellar resolution limit defines the lower bound (our lowest mass star particles are $216 M_{\odot}$). With the caveat that we are now likely incomplete, we repeat the fit including all halos with stars and find that the slope of the scatter from Eqn. 1 increases to $\gamma = -0.48$. This increased scatter is shown by the green band in the left panel of Figure 3.

3.1.3 All Halos

Next we extend the discussion to include dark halos. In Figure 1 we show dark halos by arbitrarily setting their stellar mass to $1 M_{\odot}$, so that they pile up along $\log(M_{star}) = 0$. We quantify the fraction of halos that are occupied by any stars (i.e., contain one or more star particles) as a function of halo mass in Figure 4. We note that baryonic physics can impact halo mass, lowering the final M_{halo} of a given galaxy in the baryonic run from the corresponding halo run with dark matter only. As was mentioned above, the well-resolved halos in Figure 1 use halo masses from a dark matter-only run for consistency with derived SMHM relations; Figure 4 demonstrates why. The left plot of Figure 4 shows the cumulative halo mass functions for both the baryonic and dark matter-only versions of the 40 Thieves. The solid and dashed lines trace all halos, regardless of whether they contain stars. It can be seen that the mass functions of the two runs do not quite match. This mismatch is due to the fact that in the baryonic run the ejection of baryons from low mass halos (either by heating from the UV background or as a result of supernova feedback) reduces the growth rate of a halo. The overall effect is that a given halo in the baryonic run is less

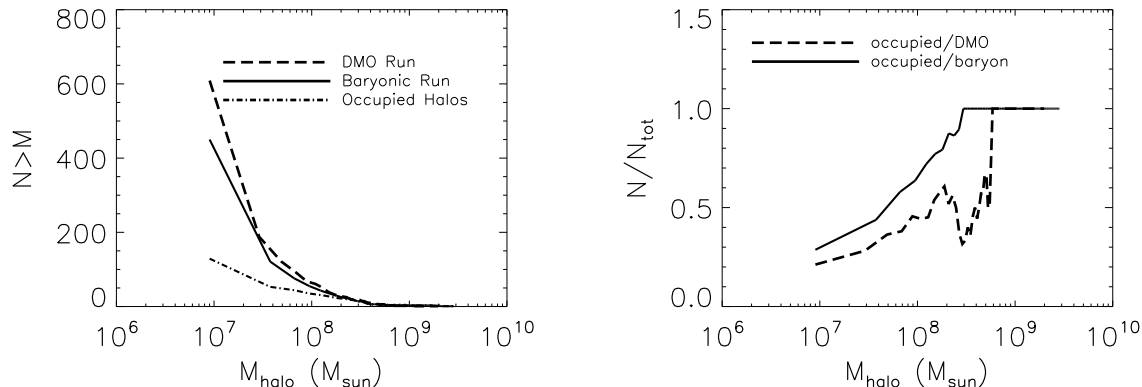


Figure 4. *Cumulative halo mass functions.* Left Panel: The dashed line is the cumulative mass function for the dark matter-only (DMO) run; the solid line is the cumulative mass function for the baryonic run using all halos; the dot-dashed line the cumulative mass function using only occupied (luminous, with a minimum of one star particle) halos in the baryonic run. Right Panel: The ratio of the cumulative number of occupied (luminous) halos relative to the corresponding number of halos in the DMO run (dashed line) and the baryon run (solid line). The fraction of dark (non-luminous) halos increases with decreasing halo mass.

massive than in the corresponding dark matter-only simulation (see also Sawala et al. 2013; Munshi et al. 2013). As a direct result, the total number of halos with $M_{halo} > 10^7 M_{\odot}$ is reduced ($\sim 75\%$) in the baryonic run compared to the dark matter-only run. Figure 4 also shows the cumulative mass function for only those halos that “host a galaxy,” i.e., contain a minimum of one star particle (see also Sawala et al. 2015).

In the right panel of Figure 4, we plot the ratio between the number of occupied halos (that contain one or more star particle) to the total number of halos in both the dark matter-only and baryonic simulations. At halo masses of $10^7 M_{\odot}$, only 20% of halos are occupied compared to the number of halos in the dark matter-only run. Due to the fact that the baryonic run contains fewer halos at $10^7 M_{\odot}$, the fraction is slightly higher relative to the baryonic run; luminous halos compose 30% of the total number of halos with masses above $10^7 M_{\odot}$ in the baryonic run.

Hence, in the presence of baryons, Λ CDM predicts a significant number of dark halos at very low mass. We attempt to recalculate the scatter and slope of the SMHM when these halos with $M_{star} = 0 M_{\odot}$ are considered. We do this not to redefine the definition of a galaxy (Willman & Strader 2012), but purely as a demonstration of how the scatter in the relationship grows if dark halos are included. We note that log-normal scatter is technically no longer a good description of the relation, as there are more dark halos than luminous halos below $M_{halo} \sim 10^8 M_{\odot}$, and the scatter is no longer evenly distributed above and below the mean. However, if we ignore that fact and use Eqn. 1 including all halos, we find that the rate at which scatter grows increases drastically, resulting in a slope $\gamma = -0.85$. The slope at the low mass end of the relation also steepens below $\log(M_{halo}) = 8.4$, to $\alpha = 0.84$. The increased scatter including the dark halos is shown in the left hand panel of Figure 3 by the yellow band. As with the well-resolved halos, the scatter above halo masses of $10^9 M_{\odot}$ remains 0.1 dex, as there are no dark halos in this mass range. The scatter increases to 0.8 dex at

a halo mass of $10^8 M_{\odot}$, and to 2.4 dex at a halo mass of $10^7 M_{\odot}$.

3.2 Populating a Halo Mass Function

We demonstrate in this subsection how to reproduce our results given a halo mass function. The contours in the left panel of Figure 5 shows the results of stochastically populating 200,000 halos below $\log(M_{halo}) = 11.5$ given a halo mass function in our WMAP3 cosmology. We wish to reproduce the general trends seen in the black points, which are the same as the grey points in Figure 1, but we also assume there may be real galaxies that host stellar populations below our resolution limit of one star particle. To populate our halos, we adopt the log-normal scatter for the well-resolved halos, but we simultaneously require that the fraction of luminous galaxies (i.e., the fraction of galaxies with stellar masses above our resolution limit) matches the results in the right hand panel of Figure 4. Recall that for our well-resolved halos, a slope of the SMHM $\alpha = 2.4$ is the best fit for $8.4 < \log(M_{halo}) < 11.5$, with a shallower slope of $\alpha = 0.64$ at lower halo masses. The scatter is constant at 0.2 dex above $M_1 = 5 \times 10^9 M_{\odot}$, and linearly grows below this halo mass, i.e., $\gamma = -0.26$. Once populated in halo and stellar mass, the points are binned into a 2D histogram, which is normalized such that the total volume of the histogram is unity. Resulting contours of constant density from this histogram are plotted in Figure 5.

The right panel of Figure 5 shows the resulting stellar mass function after populating 200,000 halos. Garrison-Kimmel et al. (2016) recently demonstrated that large scatter impacts the observed stellar mass function. Due to the rapidly rising halo mass function, halos are more likely to scatter to larger stellar masses, an effect that is increasingly noticeable as scatter increases. Our scatter grows in such a way that it only reaches relatively large scatter (~ 1 dex) at very low halo masses that host primarily ultra-faint galaxies. Thus, the scatter only has a noticeable impact on the stellar mass function at masses

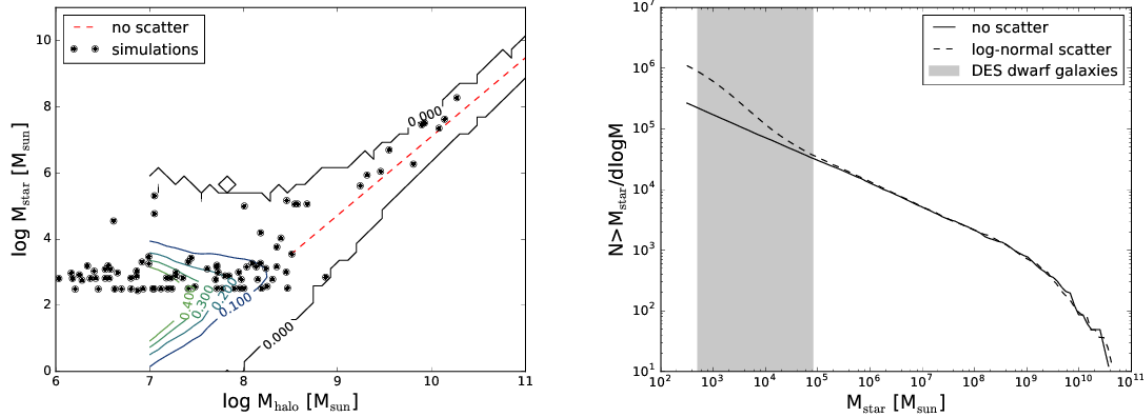


Figure 5. *Populating a Halo Mass Function Including Scatter.* Left Panel: The black points are the same as the grey in Figure 1. The constant-density contours are the 2D probability density function resulting from stochastically populating 200,000 halos with log-normal scatter below $\log(M_{\text{halo}}) = 11.5$, while requiring that the fraction of dark halos (i.e., those below our resolution limit of 1 star particle) reproduces the results in the right panel of Figure 4 as a function of halo mass. We adopt the trends defined for our well-resolved halos: a slope of the SMHM $\alpha = 2.4$ for $8.4 < \log(M_{\text{halo}}) < 11.5$ (shown by the red dashed line), with a shallower slope of $\alpha = 0.64$ at lower halo masses. The scatter is fixed to a constant 0.2 above $M_1 = 5 \times 10^9 M_{\odot}$, and linearly grows below this halo mass so that $\gamma = -0.26$. Adopting these criteria generally reproduces our SMHM relation results. Right panel: The change in the stellar mass function including scatter (dashed line). We compare to the case with no scatter (solid line). The scatter is small enough at high halo masses to have almost no impact on the resulting mass function. It is not until the scatter grows to nearly 1 dex at the smallest halo masses ($10^7 M_{\odot}$) that the scatter begins to alter the stellar mass function. This change falls in the range of masses of the recently discovered DES dwarfs (shaded region).

below $\sim 10^4 M_{\odot}$. These are luminosities below which the observed luminosity or stellar mass function are not currently complete, but are being or will be probed by surveys like DES, HSC-SSP, or with LSST (Tollerud et al. 2008; Walsh, Willman & Jerjen 2009). In the right panel of Figure 5, we shade the mass region of the new dwarf satellites that have been found in the first two years of the DES (Bechtol et al. 2015; Drlica-Wagner et al. 2015).

Despite the fact that the stellar mass function is not altered in the current range that is observationally complete, the stochastic nature of star formation in low mass dwarfs is still significant, leading to an increasingly steep slope at soon-to-be probed masses. Tollerud et al. (2008) estimates that such faint dwarf galaxies should be observed out to ~ 1 Mpc by LSST after the full co-added data are collected. Thus, our predicted increase in the slope of the stellar mass function can be tested.

3.3 Star Formation Model

The star formation prescription used in this work adopts a high density threshold for star formation ($\rho > 100$ amu/cc, $T < 10^4$ K), which has been shown to produce resolved stellar populations as seen in real dwarfs (Governato et al. 2015). However, Christensen et al. (2014) demonstrated that gas that is restricted to forming from molecular (H_2) gas forms at even higher densities and colder temperatures. This change does not affect our SMHM results for halos more massive than $\sim 10^8 M_{\odot}$, because our results in this work at the high mass end are in agreement with Munshi et al. (2013), who examined the SMHM using simulated galaxies in which stars formed only in the presence of H_2 (Christensen et al. 2012).

However, it is not clear that our results at lower masses would also remain unchanged if we adopted an H_2 -based star formation prescription, particularly for the halos that form only one star particle. Current observations are incomplete in the ultra-faint dwarf galaxy luminosity range. If a change in the star formation prescription yields different results at the low mass end, this could result in a different prediction for the stellar mass function. This is unlikely, as our predictions are based off of the scatter in our well-resolved halos, which also form stars at the high densities achieved when H_2 star formation is followed.

Despite these caveats, in a future work we will examine the differences in the SMHM relation at lower masses that result from restricting stars to forming in even higher density gas (Munshi et al., *in prep*). Studying differences in star formation in the lowest mass halos has multiple implications. First, any difference in the stellar mass function between the two models means that the observed stellar mass function from LSST at ultra-faint dwarf scales can constrain star formation models. Second, changes in star formation at the lowest masses will alter predictions for how many faint satellites will be observed around dwarf galaxies (Sales et al. 2013; Wheeler et al. 2015; Dooley et al. 2016, 2017). We will make predictions for each of these observations in the two different star formation models (Munshi et al., *in prep*).

4 SUMMARY

In this paper, we use a large sample of extremely high resolution simulated dwarf field galaxies (SMC-mass and smaller) and their satellites in order to predict the SMHM relation at low halo masses. This is the first prediction of the SMHM relation for field galaxies down to $M_{\text{halo}} = 10^7 M_{\odot}$, and the

first time that the scatter at the low mass end has been robustly quantified. We demonstrate that (1) derived SMHM relations cannot be extrapolated from higher masses to lower masses, and thus (2) the halo mass of a faint dwarf galaxy cannot be inferred *a priori*.

We quantify the scatter both in terms of scatter in halo mass given a stellar mass and scatter in stellar mass for a given halo mass. We show that scatter increases dramatically for lower-mass halos. When we consider only well-resolved simulated halos above $10^7 M_\odot$ (i.e., those that contain more than 1500 particles and that are above the hydrogen cooling limit), the scatter in M_{star} at $M_{halo} \sim 10^7 M_\odot (z = 0)$ reaches values as large as ~ 1 dex. Assuming log-normal scatter, the rate of increase in scatter is quantified by γ , where $\gamma = -0.26$ for well-resolved halos.

For the first time, we also demonstrate that much of this scatter is due to the inclusion of satellite galaxies in the SMHM relation. For our well-resolved halos, considering the maximum halo mass achieved by our satellites decreases the scatter in the SMHM from ~ 1 dex to ~ 0.25 dex at a halo mass of $10^7 M_\odot$. The origin of this scatter is the fact that the satellites of our dwarf galaxies can lose substantial mass after infall, including satellites that lose an order of magnitude or more in halo mass.

The substantial stripping that some of our satellites of dwarfs experience may run counter to naive expectations that tidal mass loss is inconsequential in the shallow potential wells of dwarf galaxies. In a future work (Ahmed et al., *in prep*), we will examine the mass loss of these dwarf galaxy satellites in more detail. It has been suggested that some of the recently discovered DES dwarfs may be satellites of the Magellanic Clouds D’Onghia & Lake (2008); Deason et al. (2015); Yozin & Bekki (2015); Jethwa, Erkal & Belokurov (2016); Dooley et al. (2017); Sales et al. (2017), as associations of dwarf galaxies and their satellites are a natural outcome of CDM (Stierwalt et al. 2017), and could be responsible for many of the ultrafaint dwarfs in the MW halo. None of these works have highlighted that the satellites of dwarfs may be substantially stripped, which has implications for their expected velocity dispersions.

However, the majority of halos with $10^7 < M_{halo}/M_\odot < 10^8$ have no galaxy associated with them. They are dark halos. Using the strictest definition possible (no star particles formed in the simulated halo), we derive the fraction of dark halos at a given halo mass. By including our estimate of the fraction of dark halos and the scatter of our well-resolved halos, we have provided a tool that can be used to stochastically populate theoretical models at low masses instead of relying on abundance matching. We demonstrate this by populating a halo mass function including the scatter for our well-resolved halos, and requiring that we reproduce the fraction of dark halos in the simulation as a function of halo mass. The resulting stellar mass function is steepened in the mass range of ultra-faint dwarfs due to the large scatter in stellar mass at low halo masses, which places higher stellar mass into some low mass halos. This luminosity/mass range is currently being probed by surveys like DES, which has discovered 16 new ultra-faint dwarfs in its first two years (Bechtol et al. 2015; Drlica-Wagner et al. 2015), and the HSC-SSP, which has already discovered one new dwarf (Homma et al. 2017). Additional dwarfs should be discovered by LSST when it comes online, allowing the

stellar mass function in this range to be probed observationally.

Most importantly, the large scatter in our simulated SMHM demonstrates that the commonly-adopted assumption of a monotonic relationship between stellar mass and halo mass that is adopted in abundance matching breaks down at low masses. At the faintest end of the SMHM probed by our simulations, a galaxy cannot be assigned a unique halo mass based solely on its stellar mass or luminosity. In the regime $M_{star}(z = 0) \lesssim 10^6 M_\odot (M_V \sim -8)$, dark matter halo masses may vary by a factor of 100 at a fixed stellar mass. Thus, abundance matching of galaxies below $M_{star} = 10^6 M_\odot$ must consider the effect of large scatter.

The lack of a monotonic relation between stellar mass and halo mass has implications for interpreting observations of dwarf galaxies. SMHM relations derived at higher masses cannot be extrapolated to infer the mass of a faint dwarf. Instead, each faint galaxy must be regarded individually, using kinematics to infer halo mass. Additionally, if a faint galaxy can be residing in a range of halo masses, it is no longer sufficient to assume a faint galaxy has been quenched by reionization. Rather, the halo mass in which the dwarf resides (or originally resided in, in the case of satellites) that matters. By providing a model to stochastically populate the low mass halo function, we have opened the door to allow these issues to be studied more realistically.

ACKNOWLEDGEMENTS

FDM acknowledges support from the Vanderbilt Initiative for Data-Intensive Astrophysics (VIDA) through a VIDA Postdoctoral Fellowship, from the University of Oklahoma, and from HST AR-13925 provided by NASA through a grant from the Space Telescope Science Institute, which is operated by the Association of Universities for Research in Astronomy, Incorporated, under NASA contract NAS5-26555. FG and TRQ were partially supported by NSF award AST-1311956 and HST award AR-13264. FG was partially supported by NSF AST-1410012, HST AR-14281, and NASA NNX15AB17G. This research is part of the Blue Waters sustained-petascale computing project, which is supported by the National Science Foundation (awards OCI-0725070 and ACI-1238993) and the state of Illinois. Blue Waters is a joint effort of the University of Illinois at Urbana-Champaign and its National Center for Supercomputing Applications. This work is also part of a PRAC allocation support by the National Science Foundation (award number OCI-1144357). The authors thank Shea Garrison-Kimmel, Kelly Holley-Bockelmann, Michael Tremmel and Adi Zolotov for assistance and helpful comments.

References

- Agertz O., Kravtsov A. V., Leitner S. N., Gnedin N. Y., 2013, *The Astrophysical Journal*, 770, 25
- Aumer M., White S. D. M., Naab T., Scannapieco C., 2013, *Monthly Notices of the Royal Astronomical Society*, 434, 3142

- Barnes J., Efstathiou G., 1987, *The Astrophysical Journal*, 319, 575
- Bechtol K. et al., 2015, *The Astrophysical Journal*, 807, 50
- Behroozi P. S., Wechsler R. H., Conroy C., 2013, *The Astrophysical Journal*, 770, 57
- Brook C. B., Di Cintio A., 2015, *Monthly Notices of the Royal Astronomical Society*, 450, 3920
- Brook C. B., Di Cintio A., Knebe A., Gottlöber S., Hoffman Y., Yepes G., Garrison-Kimmel S., 2014, *The Astrophysical Journal Letters*, 784, L14
- Brook C. B. et al., 2011, *Monthly Notices of the Royal Astronomical Society*, 415, 1051
- Brook C. B., Stinson G., Gibson B. K., Wadsley J., Quinn T., 2012, *Monthly Notices of the Royal Astronomical Society*, 424, 1275
- Brooks A., Christensen C., 2016, *Galactic Bulges*, 418, 317
- Brooks A. M., Governato F., Booth C. M., Willman B., Gardner J. P., Wadsley J., Stinson G., Quinn T., 2007, *The Astrophysical Journal Letters*, 655, L17
- Brooks A. M., Kuhlen M., Zolotov A., Hooper D., 2013, *The Astrophysical Journal*, 765, 22
- Brooks A. M., Papastergis E., Christensen C. R., Governato F., Stilp A., Quinn T. R., Wadsley J., 2017, *ArXiv e-prints*
- Brooks A. M., Zolotov A., 2014, *The Astrophysical Journal*, 786, 87
- Brown T. M. et al., 2012, *The Astrophysical Journal Letters*, 753, L21
- Brown T. M. et al., 2014, *The Astrophysical Journal*, 796, 91
- Bryan G. L., Norman M. L., 1998, *The Astrophysical Journal*, 495, 80
- Chang J., Macciò A. V., Kang X., 2013, *Monthly Notices of the Royal Astronomical Society*, 431, 3533
- Christensen C., Quinn T., Governato F., Stilp A., Shen S., Wadsley J., 2012, *Monthly Notices of the Royal Astronomical Society*, 425, 3058
- Christensen C. R., Davé R., Governato F., Pontzen A., Brooks A., Munshi F., Quinn T., Wadsley J., 2016, *The Astrophysical Journal*, 824, 57
- Christensen C. R., Governato F., Quinn T., Brooks A. M., Shen S., McCleary J., Fisher D. B., Wadsley J., 2014, *Monthly Notices of the Royal Astronomical Society*, 440, 2843
- Conroy C., Wechsler R. H., 2009, *The Astrophysical Journal*, 696, 620
- Deason A. J., Wetzel A. R., Garrison-Kimmel S., Belokurov V., 2015, *Monthly Notices of the Royal Astronomical Society*, 453, 3568
- Di Cintio A., Brook C. B., Macciò A. V., Stinson G. S., Knebe A., Dutton A. A., Wadsley J., 2014, *Monthly Notices of the Royal Astronomical Society*, 437, 415
- D’Onghia E., Lake G., 2008, *The Astrophysical Journal Letters*, 686, L61
- Dooley G. A., Peter A. H. G., Carlin J. L., Frebel A., Bechtol K., Willman B., 2017, *ArXiv e-prints*
- Dooley G. A., Peter A. H. G., Yang T., Willman B., Griffen B. F., Frebel A., 2016, *ArXiv e-prints*
- Drlica-Wagner A. et al., 2016, *The Astrophysical Journal Letters*, 833, L5
- Drlica-Wagner A. et al., 2015, *The Astrophysical Journal*, 813, 109
- Ferrero I., Abadi M. G., Navarro J. F., Sales L. V., Gurovich S., 2012, *Monthly Notices of the Royal Astronomical Society*, 425, 2817
- Fitts A. et al., 2016, *ArXiv e-prints*
- Garrison-Kimmel S., Boylan-Kolchin M., Bullock J. S., Kirby E. N., 2014a, *Monthly Notices of the Royal Astronomical Society*, 444, 222
- Garrison-Kimmel S., Boylan-Kolchin M., Bullock J. S., Lee K., 2014b, *Monthly Notices of the Royal Astronomical Society*, 438, 2578
- Garrison-Kimmel S., Bullock J. S., Boylan-Kolchin M., Bardwell E., 2016, *ArXiv e-prints*
- Gill S. P. D., Knebe A., Gibson B. K., 2004, *Monthly Notices of the Royal Astronomical Society*, 351, 399
- Girardi L. et al., 2010, *The Astrophysical Journal*, 724, 1030
- Gnedin N. Y., 2000, *The Astrophysical Journal*, 535, 530
- Governato F. et al., 2010, *Nature*, 463, 203
- Governato F. et al., 2015, *Monthly Notices of the Royal Astronomical Society*, 448, 792
- Governato F., Willman B., Mayer L., Brooks A., Stinson G., Valenzuela O., Wadsley J., Quinn T., 2007, *Monthly Notices of the Royal Astronomical Society*, 374, 1479
- Governato F. et al., 2012, *Monthly Notices of the Royal Astronomical Society*, 422, 1231
- Guo Q., White S., Li C., Boylan-Kolchin M., 2010, *Monthly Notices of the Royal Astronomical Society*, 404, 1111
- Haardt F., Madau P., 2012, *The Astrophysical Journal*, 746, 125
- Homma D. et al., 2017, *ArXiv e-prints*
- Hopkins P. F., Keres D., Onorbe J., Faucher-Giguere C.-A., Quataert E., Murray N., Bullock J. S., 2013, *ArXiv e-prints*
- Jethwa P., Erkal D., Belokurov V., 2016, *Monthly Notices of the Royal Astronomical Society*, 461, 2212
- Katz N., White S. D. M., 1993, *The Astrophysical Journal*, 412, 455
- Keller B. W., Wadsley J., Benincasa S. M., Couchman H. M. P., 2014, *Monthly Notices of the Royal Astronomical Society*, 442, 3013
- Kim D., Jerjen H., 2015, *The Astrophysical Journal Letters*, 808, L39
- Kim D., Jerjen H., Mackey D., Da Costa G. S., Milone A. P., 2015, *The Astrophysical Journal Letters*, 804, L44
- Kim J.-h. et al., 2014, *The Astrophysical Journal Supplement*, 210, 14
- Klypin A., Karachentsev I., Makarov D., Nasonova O., 2015, *Monthly Notices of the Royal Astronomical Society*, 454, 1798
- Knollmann S. R., Knebe A., 2009, *The Astrophysical Journal Supplement*, 182, 608
- Koposov S. E., Belokurov V., Torrealba G., Evans N. W., 2015, *The Astrophysical Journal*, 805, 130
- Kravtsov A., Vikhlinin A., Meshcheryakov A., 2014, *ArXiv e-prints*
- Laevens B. P. M. et al., 2015, *The Astrophysical Journal*, 813, 44
- Libeskind N. I., Knebe A., Hoffman Y., Gottlöber S., Yepes G., 2011, *Monthly Notices of the Royal Astronomical Society*, 418, 336
- Luque E. et al., 2017, *Monthly Notices of the Royal Astronomical Society*, 468, 97

- Marigo P., Girardi L., Bressan A., Groenewegen M. A. T., Silva L., Granato G. L., 2008, *Astronomy & Astrophysics*, 482, 883
- Marinacci F., Pakmor R., Springel V., 2014, *Monthly Notices of the Royal Astronomical Society*, 437, 1750
- Martin N. F. et al., 2015, *The Astrophysical Journal Letters*, 804, L5
- Matthee J., Schaye J., Crain R. A., Schaller M., Bower R., Theuns T., 2017, *Monthly Notices of the Royal Astronomical Society*, 465, 2381
- Maxwell A. J., Wadsley J., Couchman H. M. P., 2015, *The Astrophysical Journal*, 806, 229
- Menon H., Wesolowski L., Zheng G., Jetley P., Kale L., Quinn T., Governato F., 2015, *Computational Astrophysics and Cosmology*, 2, 1
- Moster B. P., Naab T., White S. D. M., 2013, *Monthly Notices of the Royal Astronomical Society*, 428, 3121
- Muñoz R. R., Majewski S. R., Johnston K. V., 2008, *The Astrophysical Journal*, 679, 346
- Munshi F., Christensen C., Quinn T. R., Governato F., Wadsley J., Loebman S., Shen S., 2014, *The Astrophysical Journal Letters*, 781, L14
- Munshi F. et al., 2013, *The Astrophysical Journal*, 766, 56
- Oñorbe J., Boylan-Kolchin M., Bullock J. S., Hopkins P. F., Kereš D., Faucher-Giguère C.-A., Quataert E., Murray N., 2015, *Monthly Notices of the Royal Astronomical Society*, 454, 2092
- Okamoto T., Gao L., Theuns T., 2008, *Monthly Notices of the Royal Astronomical Society*, 390, 920
- Oppenheimer B. D., Davé R., Kereš D., Fardal M., Katz N., Kollmeier J. A., Weinberg D. H., 2010, *Monthly Notices of the Royal Astronomical Society*, 406, 2325
- O’Shea B. W., Wise J. H., Xu H., Norman M. L., 2015, *The Astrophysical Journal Letters*, 807, L12
- Papastergis E., Giovanelli R., Haynes M. P., Shankar F., 2015, *Astronomy & Astrophysics*, 574, A113
- Peñarrubia J., McConnachie A. W., Navarro J. F., 2008, *The Astrophysical Journal*, 672, 904
- Pontzen A. et al., 2010, *Monthly Notices of the Royal Astronomical Society*, 402, 1523
- Pontzen A., Governato F., 2014, *Nature*, 506, 171
- Pontzen A. et al., 2008, *Monthly Notices of the Royal Astronomical Society*, 390, 1349
- Pontzen A., Roškar R., Stinson G., Woods R., 2013, *pynbody: N-Body/SPH analysis for python*. *Astrophysics Source Code Library*
- Read J. I., Agertz O., Collins M. L. M., 2016, *Monthly Notices of the Royal Astronomical Society*, 459, 2573
- Read J. I., Iorio G., Agertz O., Fraternali F., 2017, *Monthly Notices of the Royal Astronomical Society*, 467, 2019
- Reddick R. M., Wechsler R. H., Tinker J. L., Behroozi P. S., 2013, *The Astrophysical Journal*, 771, 30
- Sales L. V., Navarro J. F., Kallivayalil N., Frenk C. S., 2017, *Monthly Notices of the Royal Astronomical Society*, 465, 1879
- Sales L. V., Wang W., White S. D. M., Navarro J. F., 2013, *Monthly Notices of the Royal Astronomical Society*, 428, 573
- Sawala T., Frenk C. S., Crain R. A., Jenkins A., Schaye J., Theuns T., Zavala J., 2013, *Monthly Notices of the Royal Astronomical Society*, 431, 1366
- Sawala T. et al., 2015, *Monthly Notices of the Royal Astronomical Society*, 448, 2941
- Sawala T. et al., 2016, *Monthly Notices of the Royal Astronomical Society*, 456, 85
- Shen S., Madau P., Conroy C., Governato F., Mayer L., 2014, *The Astrophysical Journal*, 792, 99
- Shen S., Wadsley J., Stinson G., 2010, *Monthly Notices of the Royal Astronomical Society*, 407, 1581
- Simpson C. M., Bryan G. L., Johnston K. V., Smith B. D., Mac Low M.-M., Sharma S., Tumlinson J., 2013, *Monthly Notices of the Royal Astronomical Society*, 432, 1989
- Stierwalt S., Liss S. E., Johnson K. E., Patton D. R., Privon G. C., Besla G., Kallivayalil N., Putman M., 2017, *Nature Astronomy*, 1, 0025
- Stinson G., Seth A., Katz N., Wadsley J., Governato F., Quinn T., 2006, *Monthly Notices of the Royal Astronomical Society*, 373, 1074
- Stinson G. S., Brook C., Macciò A. V., Wadsley J., Quinn T. R., Couchman H. M. P., 2013, *Monthly Notices of the Royal Astronomical Society*, 428, 129
- Strigari L. E., Bullock J. S., Kaplinghat M., Simon J. D., Geha M., Willman B., Walker M. G., 2008, *Nature*, 454, 1096
- Tollerud E. J., Bullock J. S., Strigari L. E., Willman B., 2008, *The Astrophysical Journal*, 688, 277
- Torrealba G. et al., 2016, *Monthly Notices of the Royal Astronomical Society*, 463, 712
- Walsh S. M., Willman B., Jerjen H., 2009, *The Astronomical Journal*, 137, 450
- Wechsler R. H., Bullock J. S., Primack J. R., Kravtsov A. V., Dekel A., 2002, *The Astrophysical Journal*, 568, 52
- Weisz D. R., Dolphin A. E., Skillman E. D., Holtzman J., Gilbert K. M., Dalcanton J. J., Williams B. F., 2014, *The Astrophysical Journal*, 789, 148
- Weisz D. R., Dolphin A. E., Skillman E. D., Holtzman J., Gilbert K. M., Dalcanton J. J., Williams B. F., 2015, *The Astrophysical Journal*, 804, 136
- Wheeler C., Oñorbe J., Bullock J. S., Boylan-Kolchin M., Elbert O. D., Garrison-Kimmel S., Hopkins P. F., Kereš D., 2015, *Monthly Notices of the Royal Astronomical Society*, 453, 1305
- Willman B., Strader J., 2012, *The Astronomical Journal*, 144, 76
- Yozin C., Bekki K., 2015, *Monthly Notices of the Royal Astronomical Society*, 453, 2302
- Zhao D. H., Jing Y. P., Mo H. J., Börner G., 2003, *The Astrophysical Journal Letters*, 597, L9